International Journal of Bifurcation and Chaos

PERIODICALLY FORCED PIECEWISE LINEAR ADAPTIVE EXPONENTIAL INTEGRATE-AND-FIRE NEURON

LIEJUNE SHIAU
Department of Mathematics
University of Houston, Clear Lake
Houston TX 77058, USA
shiau@uhcl.edu

CARLO R. LAING
Institute of Information
and Mathematical Sciences
Massey University
Private Bag 102-904, NSMC
Auckland, New Zealand
c.r.laing@massey.ac.nz

Received (to be inserted by publisher)

Although variability is a ubiquitous characteristic of the nervous system, under appropriate conditions neurons can generate precisely timed action potentials. Thus considerable attention has been given to the study of a neuron's output in relation to its stimulus. In this study, we consider an increasingly popular spiking neuron model, the adaptive exponential integrate-and-fire neuron. For analytical tractability, we consider its piecewise linear variant in order to understand the responses of such neurons to periodic stimuli. There exist regions in parameter space in which the neuron is mode locked to the periodic stimulus, and instabilities of the mode locked states lead to an Arnol'd tongue structure in parameter space. We analyze mode locked solutions and examine the bifurcations that define the boundaries of the tongue structures. The theoretical analysis is in excellent agreement with numerical simulations, and this study can be used to further understand the functional features related to responses of such a model neuron to biologically realistic inputs.

Keywords: periodic stimuli; mode locked solutions; Arnol'd tongue; piecewise-linear adaptive exponential integrate-and-fire neuron

1. Introduction

Frequency selectivity in the form of mode locking has been shown in stimulated nervous systems, such as complex sounds in the auditory nerve [Moller, 1983], hair cells in amphibian cochlea [Koch, 1999], and thalamocortical relay neuron response [Smith *et al.*, 2000; Knight, 1972; McCormick & Huguenard, 1992]. To understand the mechanisms behind these phenomena, spiking neuron models have been used to study the precise timing of firing events thought to underlie frequency mode locking [Rieke *et al.*, 1997]. Among them, various one-dimensional neuron models, such as variants of leaky integrate-and-fire model, are of particular interest for their reduced complexity. The disadvantages of these models are their limitations in

producing a variety of neuronal behaviors, and having parameters of little biophysiological relevance. On the contrary, high dimensional neuron models such as variants of the Hodgkin-Huxley model, though more capable of producing various neuronal behaviors and with biophysiologically relevant parameters, generally pose difficulty in their mathematical analysis.

In recent years substantial efforts have been exerted to develop single neuron models of reduced complexity that can produce a large repertoire of neuronal behaviors, in attempts to develop an understanding of brain function, while reducing computation demands and maintaining analytical tractability. A number of variants of two-dimensional leaky integrate-and-fire neuron models have been proposed. A popular example is the adaptive exponential leaky integrate-and-fire (aEIF) model, proposed by Brette and Gerstner [Brette & Gerstner, 2005; Gerstner & Brette, 2009], which includes a sub-threshold and a spike-triggered adaptation component in one adaptation current, and the exponential description of nearly instantaneous spike initiation. More importantly, this model's parameters are of biophysiological relevance, and its sub-threshold and spike triggered adaptation are shown to mediate spike frequency adaptation [Ladenbauer *et al.*, 2012], behaving in a way similar to a low threshold outward current, such as the muscarinic voltage-dependent K^+-current (I_m), and a high threshold outward current, such as the Ca^{2+}-dependent after-hyperpolarization K^+-current (I_{ahp}), respectively, in biophysical neuron models [Ermentrout *et al.*, 2001; Jeong & Gutkin, 2007; Ermentrout *et al.*, 2011; Ladenbauer *et al.*, 2012]. Despite its simplicity, the aEIF model can capture a broad range of neuronal dynamics [Touboul & Brette, 2008; Naud *et al.*, 2008], hence it is appropriate for applications in large-scale networks [Destexhe, 2009]. Furthermore, the aEIF model has been successfully fit to Hodgkin-Huxley-type neurons, as well as to recordings from cortical neurons [Brette & Gerstner, 2005; Clopath *et al.*, 2007; Touboul & Brette, 2008; Jolivet *et al.*, 2008]. This model has also been implemented in neuromorphic hardware systems [Brderle *et al.*, 2011], and can be tuned to reproduce the behavior of all major classes of neurons, as defined electrophysiologically in vitro [Naud *et al.*, 2008].

Based on the increasingly common use of the aEIF model, here we explore mode locked solutions, where the neuron is periodically driven by an external stimulus. To gain explicit results, we adopt the piecewise linear variant of the aEIF (PWL-aEIF) model to study these mode locked solutions. Specifically, we perform the analysis of arbitrary mode locked states for a sinosuidal external stimulus.

The work presented here is similar to that in other papers considering periodically-forced neuron models [Coombes *et al.*, 2001, 2012; Laing & Coombes, 2005; Alijani, 2009; Svensson & Coombes, 2009], however, the mode locking instabilities in this study are shown to largely be related to period-doubling of solutions and the saddle-node bifurcation of orbits which cross a particular manifold multiple times, which has not been previously observed. We first present the discontinuous differential equations describing the periodically forced PWL-aEIF neuron model. This is followed by the construction of general solutions and then the description of mode-locked solutions and their stability. We then show numerical results demonstrating our analysis, and discuss the maximal Lyapunov exponent of an arbitrary orbit. We conclude with a discussion.

2. Neuron Model

We consider a piecewise linear approximation of the adaptive exponential integrate-and-fire (PWL-aEIF) neuron [Naud *et al.*, 2008] with state variables $V(t)$ and $w(t)$ representing the cell membrane potential and adaptive current, respectively, of the neuron. (PWL neuron models have been studied a number of times over the past 10 years [Karbowski & Kopell, 2000; Coombes *et al.*, 2001; Coombes & Zachariou, 2009; Coombes *et al.*, 2012; Tonnelier, 2002].) The evolution of these variables between firing events is described according to the following equations,

$$C\frac{dV}{dt} = f(V) - w + I(t), \tag{1}$$

$$\tau_w\frac{dw}{dt} = a(V - E_L) - w, \tag{2}$$

where $f(V) = -g_L(V - E_L)$, for $V \leq V_T$, and $f(V) = g_L\Delta_T(V - E)$, for $V > V_T$, with $E = V_T + \frac{V_T - E_L}{\Delta_T}$. The function $f(V)$ is continuous and the V-nullcline, on which $dV/dt = 0$, is shown schematically in

Fig. 1 for the case $I(t) = 0$. For analytical tractability, the parameter a is set to be $a = 0$ (in (2)) in this study resulting in a horizontal w-nullcline. The physiological interpretation of the parameters is as follows [Touboul & Brette, 2008]. Eq. (1) states that the capacitive current through the membrane is the sum of the ionic currents and the injected current, $I(t)$ (C is the membrane capacitance). The term $f(V)$ represents the leak current, with g_L being the leak conductance, E_L being the leak reversal potential, and the membrane time constant being C/g_L. The V-nullcline has its minimum at $V = V_T$, and the slope factor Δ_T quantifies the sharpness of the spike. The variable w in (2) is an adaptive current with time constant τ_w, and may model ionic currents such as potassium, or a dendritic compartment. The neuron is assumed to fire whenever $V(t)$ reaches a threshold V_{th}, and then $V(t)$ is instantaneously reset to V_r and $w(t)$ is instantaneously incremented by an amount b ($b \geq 0$) as

$$\begin{cases} V(t) \mapsto V_r, \\ w(t) \mapsto w(t) + b. \end{cases}$$

We denote by $\{t_n\}_{n\in\mathbb{N}}$ the set of firing times, where $V(t_n^-) = V_{th}$ and $V(t_n^+) = V_r$.

We can further write the system (1)-(2) as

$$\dot{X} = \begin{cases} A_1 X + g_1(t), & \text{if} \quad V \leq V_T, \\ A_2 X + g_2(t), & \text{if} \quad V > V_T, \end{cases} \tag{3}$$

where $X = (V, w)^T$,

$$A_1 = \begin{bmatrix} \frac{-g_L}{C} & \frac{-1}{C} \\ 0 & \frac{-1}{\tau_w} \end{bmatrix}, \tag{4}$$

$$A_2 = \begin{bmatrix} \frac{g_L \Delta_T}{C} & \frac{-1}{C} \\ 0 & \frac{-1}{\tau_w} \end{bmatrix}, \tag{5}$$

$$g_1(t) = \begin{bmatrix} \frac{I(t)+g_L E_L}{C} \\ 0 \end{bmatrix}, \tag{6}$$

and

$$g_2(t) = \begin{bmatrix} \frac{I(t)-g_L \Delta_T E}{C} \\ 0 \end{bmatrix}. \tag{7}$$

The general solution of this type of linear system with the initial condition $X(t_0)$ is (writing $e^{At} \equiv G(t)$)

$$X(t) = G(t - t_0)X(t_0) + \int_0^{t-t_0} G(s)g(t - s)ds. \tag{8}$$

where $A \in \{A_i\}$ and $g \in \{g_i\}, i = 1, 2$. More specifically,

$$\begin{aligned} e^{A_1 t} \equiv G^1(t) &= \begin{bmatrix} e^{\frac{-g_L}{C}t} & \frac{-\tau_w(e^{\frac{-g_L}{C}t} - e^{\frac{-1}{\tau_w}t})}{C - g_L\tau_w} \\ 0 & e^{\frac{-1}{\tau_w}t} \end{bmatrix} \\ &= \begin{bmatrix} G^1_{11}(t) & G^1_{12}(t) \\ G^1_{21}(t) & G^1_{22}(t) \end{bmatrix} = \begin{bmatrix} G^1_{11}(t) & k_1(G^1_{11}(t) - G^1_{22}(t)) \\ 0 & G^1_{22}(t) \end{bmatrix}, \end{aligned} \tag{9}$$

where $k_1 = \frac{-\tau_w}{C - g_L\tau_w}$ and

$$\begin{aligned} e^{A_2 t} \equiv G^2(t) &= \begin{bmatrix} e^{\frac{g_L\Delta_T}{C}t} & \frac{-\tau_w(e^{\frac{g_L\Delta_T}{C}t} - e^{\frac{-1}{\tau_w}t})}{C + g_L\Delta_T\tau_w} \\ 0 & e^{\frac{-1}{\tau_w}t} \end{bmatrix} \\ &= \begin{bmatrix} G^2_{11}(t) & G^2_{12}(t) \\ G^2_{21}(t) & G^2_{22}(t) \end{bmatrix} = \begin{bmatrix} G^2_{11}(t) & k_2(G^2_{11}(t) - G^2_{22}(t)) \\ 0 & G^2_{22}(t) \end{bmatrix}, \end{aligned} \tag{10}$$

where $k_2 = \frac{-\tau_w}{C + g_L\Delta_T\tau_w}$, and $G^1_{22}(t) = G^2_{22}(t)$.

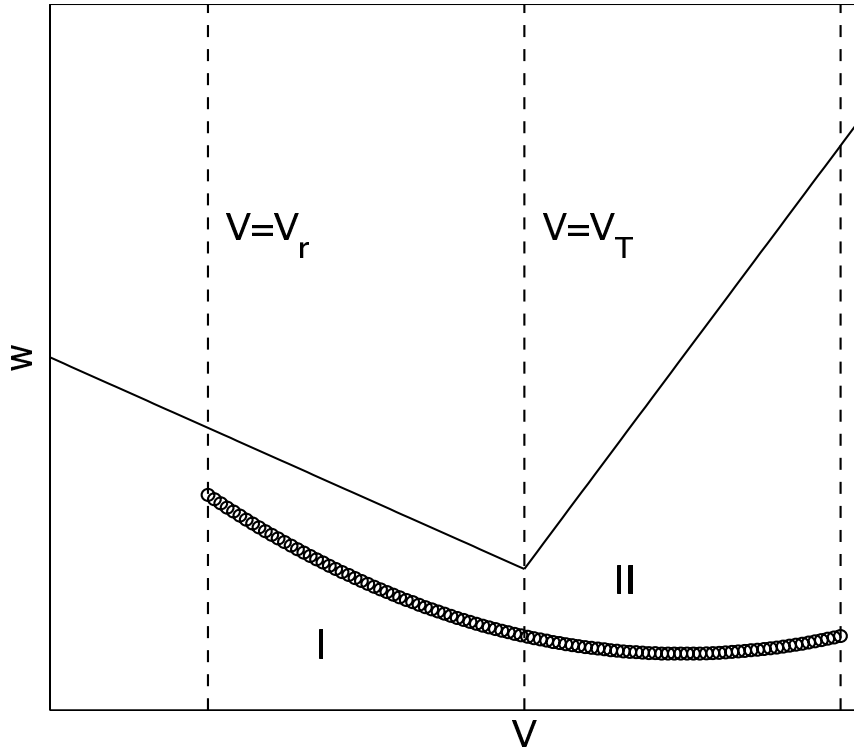

Figure 1. Schematic of the phase plane. Solid: the V-nullcline. Circles: part of a typical orbit from reset ($V = V_r$) to threshold ($V = V_{th}$) when $I(t) = 0$. Regions I ($V_r \leq V \leq V_T$) and II ($V_T < V \leq V_{th}$) are shown.

3. A General Spiking Orbit

With the PWL-aEIF system written as (3), we can construct a typical spiking orbit from a reset point (V_r, w_n) immediately after the nth spike time t_n, to the $(n+1)$th spike time (Fig. 1). After moving through region I ($V_r \leq V \leq V_T$), the orbit reaches the transition point at $(V, w) = (V_T, w(t_n + T_1^*)) \equiv (V_T, w(\hat{t}_n)) \equiv (V_T, \hat{w}_n)$, with its flight time being T_1^*. The orbit then moves through region II ($V_T < V \leq V_{th}$) and the neuron spikes when V reaches the threshold voltage at the point $(V, w) = (V_{th}, w(t_n + T_1^* + T_2^*)) = (V_{th}, w(t_{n+1}^-))$, with its flight time being T_2^*, and we have $w_{n+1} \equiv w(t_{n+1}^+) = w(t_{n+1}^-) + b$. Note that we assume that once the orbit enters region II it does not then re-enter region I, but instead leaves through the boundary $V = V_{th}$. This is not necessarily the case, as we will see later. A typical orbit from firing time t_n to t_{n+1} is formulated as follows,

$$X(t_n + T_1^*) = \begin{bmatrix} V_T \\ \hat{w}_n \end{bmatrix} \equiv G^1(T_1^*) \begin{bmatrix} V_r \\ w_n \end{bmatrix} + \int_0^{T_1^*} G^1(s) g_1(t_n + T_1^* - s) ds \tag{11}$$

and

$$X(t_n + T_1^* + T_2^*) = \begin{bmatrix} V_{th} \\ w_{n+1} - b \end{bmatrix} \equiv G^2(T_2^*) \begin{bmatrix} V_T \\ \hat{w}_n \end{bmatrix} + \int_0^{T_2^*} G^2(s) g_2(t_n + T_1^* + T_2^* - s) ds \tag{12}$$

Rewriting eqs. (11)-(12) in terms of their components, we have

$$0 = -V_T + G_{11}^1(T_1^*) V_r + G_{12}^1(T_1^*) w_n + \frac{1}{C} \int_0^{T_1^*} G_{11}^1(s) [I(t_n + T_1^* - s) + g_L E_L] ds, \tag{13}$$

$$0 = -\hat{w}_n + G_{22}^1(T_1^*) w_n, \tag{14}$$

$$0 = -V_{th} + G_{11}^2(T_2^*) V_T + G_{12}^2(T_2^*) \hat{w}_n + \frac{1}{C} \int_0^{T_2^*} G_{11}^2(s) [I(t_n + T_1^* + T_2^* - s) - g_L \Delta_T E] ds, \tag{15}$$

$$0 = -w_{n+1} + b + G_{22}^2(T_2^*) \hat{w}_n. \tag{16}$$

Solving for $w(t)$: From (14) and (16), the evolution of $w(t)$ from t_n to t_{n+1} and resetting after the firing time t_{n+1} gives

$$w_{n+1} = e^{\frac{-(t_{n+1}-t_n)}{\tau_w}} w_n + b \equiv H(t_{n+1} - t_n, w_n). \tag{17}$$

Solving for $V(t)$: The solution of $V(t)$ from t_n to t_{n+1} can be found by rewriting (13) and (15) as

$$\begin{aligned} f_1(T_1^*; t_n, w_n) =& 0 = -V_T + G_{11}^1(T_1^*)V_r + G_{12}^1(T_1^*)w_n \\ &+ \frac{1}{C}\int_0^{T_1^*} G_{11}^1(s)[I(t_n + T_1^* - s) + g_L E_L]ds, \end{aligned} \tag{18}$$

$$\begin{aligned} f_2(T_2^*; t_n, T_1^*, w_n) =& 0 = -V_{th} + G_{11}^2(T_2^*)V_T + G_{12}^2(T_2^*)G_{22}^1(T_1^*)w_n \\ &+ \frac{1}{C}\int_0^{T_2^*} G_{11}^2(s)[I(t_n + T_1^* + T_2^* - s) - g_L\Delta_T E]ds. \end{aligned} \tag{19}$$

respectively. From now on we will specify that the periodic input current is given by $I(t) = I_0 + \varepsilon\sin(\Omega t)$, where I_0 is a constant current that drives the neuron up to spike, and $\Omega = 2\pi\omega$, with ω being the input frequency. In this case f_1 and f_2 can be expressed explicitly as,

$$\begin{aligned} f_1(T_1^*; t_n, w_n) =& 0 \\ =& - V_T + e^{\frac{-g_L}{C}T_1^*}V_r + k_1(e^{\frac{-g_L}{C}T_1^*} - e^{\frac{-1}{\tau_w}T_1^*})w_n \\ &- (e^{\frac{-g_L}{C}T_1^*} - 1)(I_0 + g_L E_L)/g_L \\ &+ \frac{\varepsilon/C}{(\frac{g_L}{C})^2 + \Omega^2}\left\{-\Omega\cos(\Omega(t_n + T_1^*)) + \frac{g_L}{C}\sin(\Omega(t_n + T_1^*))\right. \\ &\left. + e^{\frac{-g_L}{C}T_1^*}\left[\Omega\cos(\Omega t_n) - \frac{g_L}{C}\sin(\Omega t_n)\right]\right\}, \end{aligned} \tag{20}$$

and

$$\begin{aligned} f_2(T_2^*; t_n, T_1^*, w_n) =& 0 \\ =& - V_{th} + e^{\frac{g_L\Delta_T}{C}T_2^*}V_T + k_2(e^{\frac{g_L\Delta_T}{C}T_2^*} - e^{\frac{-1}{\tau_w}T_2^*})e^{\frac{-1}{\tau_w}T_1^*}w_n \\ &+ (e^{\frac{g_L\Delta_T}{C}T_2^*} - 1)(I_0 - g_L\Delta_T E)/(g_L\Delta_T) \\ &+ \frac{\varepsilon/C}{(\frac{g_L\Delta_T}{C})^2 + \Omega^2}\left\{-\Omega\cos(\Omega(t_n + T_1^* + T_2^*)) - \frac{g_L\Delta_T}{C}\sin(\Omega(t_n + T_1^* + T_2^*))\right. \\ &\left. + e^{\frac{g_L\Delta_T}{C}T_2^*}\left[\Omega\cos(\Omega(t_n + T_1^*)) + \frac{g_L\Delta_T}{C}\sin(\Omega(t_n + T_1^*))\right]\right\}. \end{aligned} \tag{21}$$

We also have

$$t_{n+1} = t_n + T_1^* + T_2^*. \tag{22}$$

We can compute T_1^* by solving $f_1(T_1^*; t_n, w_n) = 0$, where t_n and w_n are specified, then compute T_2^* by solving $f_2(T_2^*; t_n, T_1^*, w_n) = 0$. The next firing time is given by (22), and w_{n+1} is computed via (17). We can thus calculate the sequence of firing times $\{t_n\}$ using (20), (21), (22) and (17), provided that the initial conditions, (t_0, w_0), are specified. Note that (20) and (21) may have more than one solution, but we solve them using a root-finder with an initial guess close to the relevant value, as found from a full simulation of (1)-(2).

We note here that the general problem of strongly-forced neurons is a difficult one to study, whereas much progress has been made in the weakly-forced (or coupled) case [Schultheiss *et al.*, 2011]. Because the model we study can be solved explicitly for all strengths of forcing, i.e. all ε, the issue as to whether forcing is weak or strong does not arise. Next we discuss mode-locked solutions and their existence.

4. Mode-locked Solutions

Instead of computing a series of firing times $\{t_n\}$ from (20), (21), (22) and (17), we describe mode-locked solutions by the phase(s) of the periodic forcing at which the neuron fires [Laing & Coombes, 2005; Coombes *et al.*, 2001]. We describe solutions for which the neuron fires p times in every q periods of the forcing function as $p:q$ mode-locked solutions, where p and q are positive integers. For such a mode-locked solution, the firing times can be expressed in terms of the firing phases as

$$t_n = \left(\lfloor n/p \rfloor + \phi_{n(p)}\right) qT, \quad n = 0, 1, 2, \cdots$$

where $\lfloor n/p \rfloor$ is the integer part of n/p, $n(p) = n \mod p$, and T is the period of the forcing ($2\pi/\Omega$). Instead of computing the firing times $\{t_n\}$, we compute the p associated firing phases $\phi_0, \cdots, \phi_{p-1} \in [0, 1)$. These distinct firing phases can be computed from (20), (21), (22) and (17), as follows.

Firstly, given q and T, we define $T_1^*(\phi_n, w_n)$ to be the solution of

$$f_1(T_1^*(\phi_n, w_n); \phi_n qT, w_n) = 0, \tag{23}$$

and $T_2^*(\phi_n, w_n)$ to be the solution of

$$f_2(T_2^*(\phi_n, w_n); \phi_n qT, T_1^*(\phi_n, w_n), w_n) = 0, \tag{24}$$

We then have, from (22) and (17),

$$\phi_{n+1} = \phi_n + \frac{T_1^*(\phi_n, w_n) + T_2^*(\phi_n, w_n)}{qT}, \tag{25}$$

$$w_{n+1} = H((\phi_{n+1} - \phi_n)qT, w_n), \tag{26}$$

for $n = 0, 1, \ldots p-1$, where $\phi_p = 1 + \phi_0$ and $w_p = w_0$. Therefore, we can find $p:q$ mode-locked solutions by simultaneously solving the $2p$ eqs. (25)-(26) for the $2p$ unknowns: $\{\phi_n\}, \{w_n\}, n = 0, 1 \ldots p-1$.

5. Stability of Mode-locked Orbits

We first discuss the evolution of perturbations to a solution using a well-established approach [Alijani, 2009; Coombes & Bressloff, 1999; Coombes, 1999; Chacron *et al.*, 2004]. For convenience, we further express the model (1)-(2) as

$$\frac{dV}{dt} = \boldsymbol{f}(V, w, t), \tag{27}$$

$$\frac{dw}{dt} = \boldsymbol{g}(w), \tag{28}$$

where

$$\boldsymbol{f}(V, w, t) = \begin{cases} [-g_L(V - E_L) - w + I_0 + \varepsilon \sin(\Omega t)]/C, & V \le V_T \\ [g_L \Delta_T (V - E) - w + I_0 + \varepsilon \sin(\Omega t)]/C, & V > V_T \end{cases}$$

and $E = V_T + (V_T - E_L)/\Delta_T$ and

$$\boldsymbol{g}(w) = -w/\tau_w,$$

with the firing rule that if $V(t^-) = V_{th}$ then $V(t^+) = V_r$ and $w(t^+) = w(t^-) + b$. Suppose we have one trajectory $(V(t), w(t))$ and a slightly perturbed trajectory $(V_p(t), w_p(t))$. We define the perturbations to be $\delta V(t) = V(t) - V_p(t)$ and $\delta w(t) = w(t) - w_p(t)$. Between firing times these perturbations evolve via

$$\frac{d}{dt}\begin{pmatrix} \delta V \\ \delta w \end{pmatrix} = \begin{pmatrix} \alpha & -1/C \\ 0 & -1/\tau_w \end{pmatrix} \begin{pmatrix} \delta V \\ \delta w \end{pmatrix} \tag{29}$$

where $\alpha = -g_L/C$, if $V \le V_T$, and $\alpha = g_L \Delta_T / C$, if $V > V_T$. Let

$$\delta X = \begin{pmatrix} \delta V \\ \delta w \end{pmatrix}.$$

That is

$$\frac{d}{dt}\delta X = \begin{cases} A_1 \delta X, & V \leq V_T \\ A_2 \delta X, & V > V_T \end{cases} \tag{30}$$

where A_1 and A_2 are (4) and (5) respectively. Suppose V reaches V_{th} at time t_1 and V_p reaches V_{th} at a later time $t_1 + \delta_1$. Then we have

$$V(t_1^-) = V_{th}, \tag{31}$$
$$V(t_1^+) = V_r, \tag{32}$$
$$V_p([t_1 + \delta_1]^-) = V_{th}, \tag{33}$$
$$V_p([t_1 + \delta_1]^+) = V_r, \tag{34}$$
$$w(t_1^+) = w(t_1^-) + b, \tag{35}$$
$$w_p([t_1 + \delta_1]^+) = w_p([t_1 + \delta_1]^-) + b. \tag{36}$$

From these we have

$$V_{th} = V_p([t_1 + \delta_1]^-) \approx V_p(t_1^-) + \delta_1 \dot{V}_p(t_1^-) \approx V_{th} - \delta V(t_1^-) + \delta_1 \dot{V}(t_1^-),$$

where an overdot indicates derivative, and thus

$$\delta_1 \approx \frac{\delta V(t_1^-)}{\dot{V}(t_1^-)} = \frac{\delta V(t_1^-)}{\boldsymbol{f}(V_{th}, w(t_1^-), t_1)}$$

Now

$$\delta V([t_1 + \delta_1]^+) = V([t_1 + \delta_1]^+) - V_p([t_1 + \delta_1]^+) \approx \delta_1 \boldsymbol{f}(V_r, w(t_1^-) + b, t_1),$$

and thus

$$\delta V([t_1 + \delta_1]^+) \approx \left[\frac{\boldsymbol{f}(V_r, w(t_1^-) + b, t_1)}{\boldsymbol{f}(V_{th}, w(t_1^-), t_1)} \right] \delta V(t_1^-).$$

We also have

$$\delta w([t_1 + \delta_1]^+) \approx \delta w(t_1^-) + \delta_1 \left[\boldsymbol{g}(w(t_1^-) + b) - \boldsymbol{g}(w(t_1^-)) \right],$$

and thus

$$\delta w([t_1 + \delta_1]^+) \approx \delta w(t_1^-) + \left[\frac{\boldsymbol{g}(w(t_1^-) + b) - \boldsymbol{g}(w(t_1^-))}{\boldsymbol{f}(V_{th}, w(t_1^-), t_1)} \right] \delta V(t_1^-).$$

Combining these into matrix form, we have

$$\begin{pmatrix} \delta V([t_1 + \delta_1]^+) \\ \delta w([t_1 + \delta_1]^+) \end{pmatrix} = \begin{pmatrix} \mathcal{A} & 0 \\ \mathcal{B} & 1 \end{pmatrix} \begin{pmatrix} \delta V(t_1^-) \\ \delta w(t_1^-) \end{pmatrix}, \tag{37}$$

where

$$\mathcal{A} \equiv \frac{\boldsymbol{f}(V_r, w(t_1^-) + b, t_1)}{\boldsymbol{f}(V_{th}, w(t_1^-), t_1)}$$

and

$$\mathcal{B} \equiv \frac{\boldsymbol{g}(w(t_1^-) + b) - \boldsymbol{g}(w(t_1^-))}{\boldsymbol{f}(V_{th}, w(t_1^-), t_1)}.$$

In the limit of $\delta_1 \to 0$, system (37) gives the contribution of the discontinuous dynamics to the evolution of the vector $\delta X = (\delta V, \delta w)^T$. Thus by integrating (30) between firing times (either analytically or numerically), and updating using (37) at each firing time, we can determine the evolution of δX and thus measure the stability of the underlying solution.

5.1. *Orbits which cross $V = V_T$ once between firing times*

We first consider the 1 : 1 locked orbit which crosses $V = V_T$ once per period. We know that w_0 is the solution of $w_0 = e^{-T/\tau_w} w_0 + b$ where T is the period of forcing. The only unknown is ϕ_0. It satisfies the scalar equation

$$T_1^*(\phi_0, w_0) + T_2^*(\phi_0, w_0) = T. \tag{38}$$

To find the orbit's stability, based on (30), which correspond to motion in regions I and II (see Fig. 1), respectively. Consider a perturbation to the solution

$$\delta X = \begin{pmatrix} \delta V \\ \delta w \end{pmatrix}$$

just after firing. At a time T_1^* after firing, this perturbation will have evolved to be $e^{A_1 T_1^*} \delta X$. After a further time T_2^* $(= T - T_1^*)$, this perturbation will be $e^{A_2 T_2^*} e^{A_1 T_1^*} \delta X$. After firing again it will be

$$\begin{pmatrix} \mathcal{A} & 0 \\ \mathcal{B} & 1 \end{pmatrix} e^{A_2 T_2^*} e^{A_1 T_1^*} \delta X,$$

where

$$\mathcal{A} \equiv \frac{\boldsymbol{f}(V_r, w_0, \phi_0 T)}{\boldsymbol{f}(V_{th}, w_0 - b, \phi_0 T)}$$

and

$$\mathcal{B} \equiv \frac{\boldsymbol{g}(w_0) - \boldsymbol{g}(w_0 - b)}{\boldsymbol{f}(V_{th}, w_0 - b, \phi_0 T)}.$$

Writing

$$D_{\phi_0} \equiv \begin{pmatrix} \mathcal{A} & 0 \\ \mathcal{B} & 1 \end{pmatrix},$$

we see that the stability of this particular solution is given by the eigenvalues of the 2×2 matrix

$$\kappa \equiv D_{\phi_0} e^{A_2 T_2^*} e^{A_1 T_1^*}. \tag{39}$$

If both eigenvalues of κ are less than one in magnitude, this 1 : 1 orbit is stable, and it will become unstable as parameters are varied if one or more of the eigenvalues leave the unit circle in the complex plane. It is also noted that, within each tongue, there are generally one stable and one unstable orbits that may emerge into a saddle-node, as I_0 varied, defining the edge of the tongue.

As an example, Fig. 2 shows the relevant eigenvalues for the pair of 1 : 1 locked orbits which cross $V = V_T$ once per period, as a function of I_0. More specially, at $I_0 = 210$, the stable orbit is associated with eigenvalues of approximately 0.6 and -0.25 (blue dots). The other unstable orbit is associated with eigenvalues of ~ 0.3 and ~ 55 (red dots). As I_0 is decreased, the stable orbit undergoes a period-doubling bifurcation (eigenvalue of -1 at $I_0 \approx 206$). As I_0 is further decreased, the stable and unstable orbits collide and go through a saddle-node bifurcation (eigenvalue of 1 at $I_0 \approx 191$). To find the value of I_0 at which the saddle-node bifurcation occurs we simultaneously solve (38) together with $\det(\kappa - I_{2\times 2}) = 0$, and to find where the period-doubling bifurcation occurs we simultaneously solve (38) together with $\det(\kappa + I_{2\times 2}) = 0$, where $I_{2\times 2}$ is the 2×2 identity matrix.

Now consider the stability of a general $p : q$ locked orbit which only crosses $V = V_T$ once every firing, with $p > 1$. The firing phases are $\phi_0, \phi_1, \ldots \phi_{p-1}$, and the values of w *after* each of these firings are $w_0, w_1, \ldots w_{p-1}$. Assume that we have found such an orbit, i.e. we know the $\{\phi_n\}$. Then

$$w_{n+1} = H((\phi_{n+1} - \phi_n) qT, w_n), \qquad n = 0, \ldots, p-2, \tag{40}$$

and $w_p = w_0$, i.e. given the phases, the $\{w_n\}$ are specified. For a given (ϕ_n, w_n), $0 \le n \le p-1$, there are two times, T_1^n and T_2^n, such that $T_2^n + T_1^n = (\phi_{n+1} - \phi_n) qT$. T_1^n is the amount of time that the solution

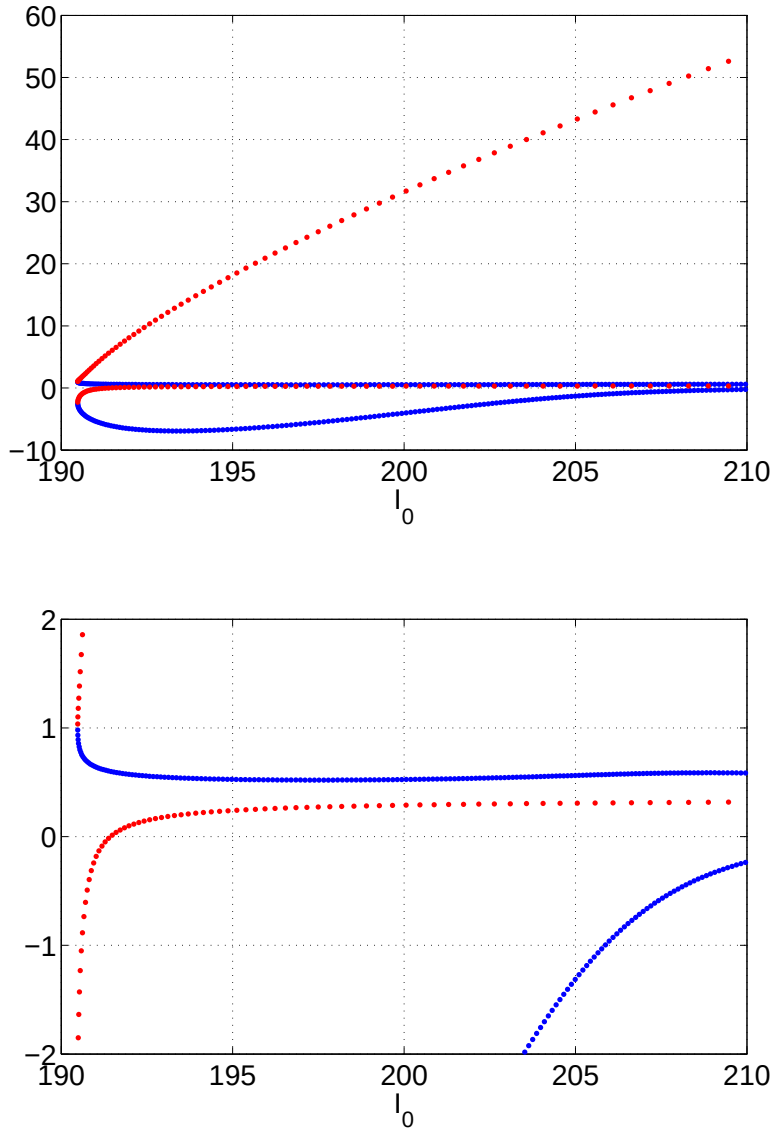

Figure 2. Eigenvalues of the two $1:1$ locked orbits which cross $V = V_T$ once per period. Blue dots are for one orbit and red for the other. The lower panel is an enlargement of the upper. Parameters: $b = 50\ pA, V_r = -60\ mV, V_{th} = -36\ mV, \tau_w = 25\ ms, C = 100\ pF, \Delta_T = 3\ mV, g_L = 10\ nS, V_T = -50\ mV, \omega = 0.04, E_L = -70\ mV, \varepsilon = 200$.

spends in region I and T_2^n is the amount of time it spends in region II, between the nth firing and the $(n+1)$th. We find T_1^n by solving

$$f_1(T_1^n, \phi_n qT, w_n) = 0,$$

and then we have $T_2^n = (\phi_{n+1} - \phi_n)qT - T_1^n$.

As above, consider a perturbation to the solution

$$\delta X = \begin{pmatrix} \delta V \\ \delta w \end{pmatrix}$$

just after firing at phase ϕ_0. After times T_1^0 and T_2^0 the perturbation has evolved to $e^{A_2 T_2^0} e^{A_1 T_1^0} \delta X$, and after firing at phase ϕ_1 the perturbation is

$$\begin{pmatrix} \mathcal{A}_1 & 0 \\ \mathcal{B}_1 & 1 \end{pmatrix} e^{A_2 T_2^0} e^{A_1 T_1^0} \delta X,$$

where

$$\mathcal{A}_1 \equiv \frac{\boldsymbol{f}(V_r, w_1, \phi_1 T)}{\boldsymbol{f}(V_{th}, w_1 - b, \phi_1 T)}$$

and

$$\mathcal{B}_1 \equiv \frac{\boldsymbol{g}(w_1) - \boldsymbol{g}(w_1 - b)}{\boldsymbol{f}(V_{th}, w_1 - b, \phi_1 T)}.$$

Writing

$$D_n \equiv \begin{pmatrix} \mathcal{A}_n & 0 \\ \mathcal{B}_n & 1 \end{pmatrix}, \qquad n = 1, \dots p,$$

where

$$\mathcal{A}_n \equiv \frac{\boldsymbol{f}(V_r, w_n, \phi_n T)}{\boldsymbol{f}(V_{th}, w_n - b, \phi_n T)}$$

and

$$\mathcal{B}_n \equiv \frac{\boldsymbol{g}(w_n) - \boldsymbol{g}(w_n - b)}{\boldsymbol{f}(V_{th}, w_n - b, \phi_n T)},$$

we see that the stability of this mode-locked solution is given by the eigenvalues of the matrix

$$\kappa \equiv \left(D_p e^{A_2 T_2^{p-1}} e^{A_1 T_1^{p-1}}\right) \times \left(D_{p-1} e^{A_2 T_2^{p-2}} e^{A_1 T_1^{p-2}}\right) \times \cdots \times \left(D_1 e^{A_2 T_2^0} e^{A_1 T_1^0}\right).$$

Note that explicit expressions for the exponentials of these matrices are given in (9) and (10).

5.2. *Orbits which cross $V = V_T$ three times between firing times*

For ε (the magnitude of the periodic forcing) large enough, V may not increase monotonically between firing times, and may cross the line $V = V_T$ several times between successive firings, as shown in Fig. 3. To identify such orbits we need to derive a new set of equations which are satisfied by these orbits. To find their stability we will need to know the amounts of time spent in the two regions, I and II.

Suppose we have a $1:1$ orbit for which the neuron fires at time t_n, then spends T_1 in region I, then T_2 in region II, then crosses $V = V_T$ from above, spending T_3 in region II before crossing again and taking time T_4 to reach V_{th} at time t_{n+1}, as shown in Fig. 3. The equations satisfied by $T_1, \dots T_4$ are given in the appendix, and using arguments similar to those above we see that the stability of such an orbit is determined by the eigenvalues of the matrix

$$\kappa \equiv D_{\phi_0} e^{A_2 T_4} e^{A_1 T_3} e^{A_2 T_2} e^{A_1 T_1}. \tag{41}$$

The parameter values at which the $1:1$ orbit transitions from crossing $V = V_T$ once per period to crossing three times per period can be found as follows. We note that immediately following firing we have

$$V(t) = F(t) \equiv e^{-g_L t/C} V_r + k_1 (e^{-g_L t/C} - e^{-t/\tau_w}) w_0 + (1/C) P(-g_L/C, t_n, t, g_L E_L), \tag{42}$$

where P is given by

$$P(a, b, c, d) \equiv \int_0^c e^{as} [I(b + c - s) + d]\, ds = (e^{ac} - 1)(I_0 + d)/a$$
$$+ \frac{\varepsilon}{a^2 + \Omega^2} \{-\Omega \cos[\Omega(b + c)] - a \sin[\Omega(b + c)] + e^{ac} [\Omega \cos(\Omega b) + a \sin(\Omega b)]\}. \tag{43}$$

We can find the first time T^* (measured from t_n) at which $V'(T^*) = 0$ by solving $F'(T^*) = 0$, where

$$CF'(t) = -g_L e^{-g_L t/C} V_r + k_1 (-g_L e^{-g_L t/C} + C e^{-t/\tau_w}/\tau_w) w_0 + P'(-g_L/C, t_n, t, g_L E_L), \tag{44}$$

where $P'(a, b, c, d) = \partial P(a, b, c, d)/\partial c$. Having found T^* the transition occurs when $F(T^*) = V_T$. Note that

$$P'(a, b, c, d) = e^{ac}(I_0 + d)$$
$$+ \frac{\varepsilon}{a^2 + \Omega^2} \{\Omega^2 \sin[\Omega(b + c)] - a\Omega \cos[\Omega(b + c)] + a e^{ac} [\Omega \cos(\Omega b) + a \sin(\Omega b)]\}. \tag{45}$$

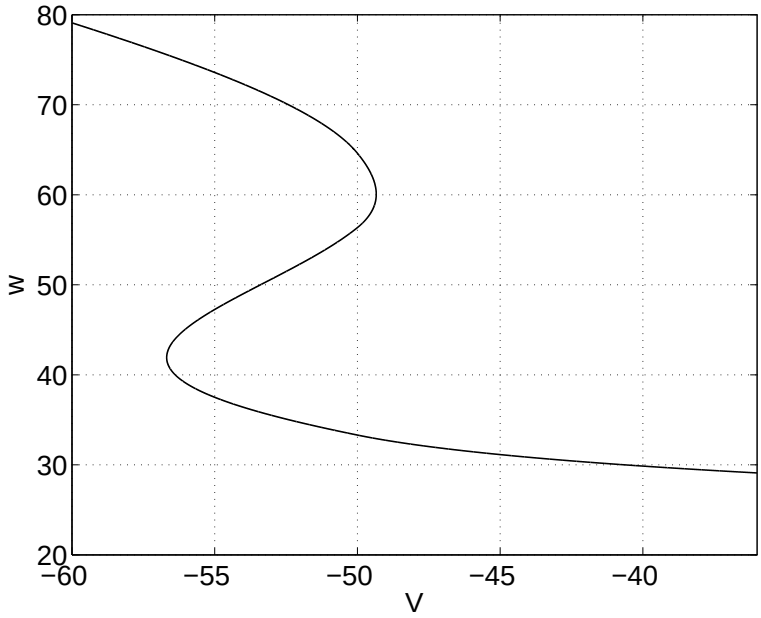

Figure 3. A $1:1$ mode locked orbit, crossing $V = V_T = -50\ mV$ three times per period. Parameters as in Fig. 2, with $I_0 = 291.6\ pA$.

Simultaneously solving the equations in the appendix for ϕ_0 and $F(T^*) = V_T$ for T^* we obtain the transition of orbits crossing $V = V_T$ once to three times per period (purple in Fig. 4). While we have only discussed this transition for the $1:1$ mode locked orbit, a similar analysis can be undertaken for any $p:q$ locked orbit.

6. Numerical Results

We now show some numerical results illustrating our analysis. Fig. 4 demonstrates the bifurcations associated with the $1:1$ orbit. Shown are the saddle-node bifurcations of the $1:1$ orbit under the assumption that $V = V_T$ once per period, the period-doubling bifurcation of this orbit, the curve on which the orbit makes the transition from crossing $V = V_T$ once per period to three times per period, and the saddle-node bifurcation of the orbit which crosses $V = V_T$ three times per period. The $1:1$ mode locked orbits are stable in the region bounded by the period-doubling curve, sn3, and the lower parts of both branches of sn1.

Numerical results for other low-order tongues are shown in Fig. 5, where only the bifurcations at which solutions lose stability are shown. We find certain features that have not been observed in some periodically forced systems studied previously. For example, in [Coombes *et al.*, 2012; Laing & Coombes, 2005; Svensson & Coombes, 2009] and [Alijani, 2009], many tongue boundaries (away from the limit of small forcing amplitude) involved non-smooth "grazing" bifurcations of the underlying flow, where a solution reaches a firing threshold tangentially. Due to the fast increase of V in region II, particularly near V_{th}, the voltage of this model neuron rises to a spike nearly instantaneously, in order to mimic more realistic neuronal spiking. Therefore, we do not observe this type of bifurcation but instead consistently see period-doubling bifurcations which mark the low-I_0 edge of tongues, and saddle-node bifurcations (of orbits which cross $V = V_T$ three times between firings) which mark the high-I_0 edge of tongues.

7. Computing the Maximal Lyapunov Exponent

Given the general analysis of the stability of an orbit in Sec. 5, we can easily find the maximal Lyapunov exponent [Coombes, 1999] associated with any orbit (not just a periodic one). In parallel with integration of the original system (1)-(2), we numerically integrate (30) between firing times, and update at firing

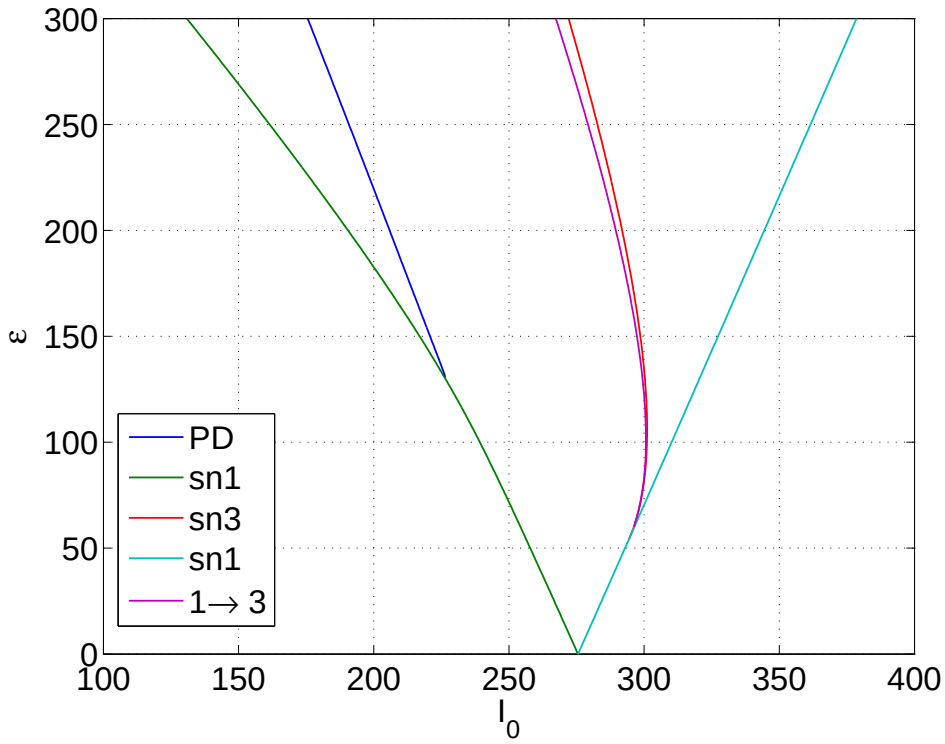

Figure 4. Bifurcations of the $1:1$ orbit. sn1: saddle-node bifurcations assuming $V = V_T$ once per period. PD: period-doubling. sn3: saddle-node bifurcation assuming $V = V_T$ three times per period. $1 \to 3$: orbit transitions from crossing $V = V_T$ once per period to three times per period. Parameters: $b = 50\ pA, V_r = -60\ mV, V_{th} = -36\ mV, \tau_w = 25\ ms, C = 100\ pF, \Delta_T = 3\ mV, g_L = 10\ nS, V_T = -50\ mV, \omega = 0.04, E_L = -70\ mV$.

times using (37). The maximal Lyapunov exponent, λ, is then defined in the usual way as

$$\lambda = \lim_{t\to\infty} \frac{1}{t} \log |\delta X(t)|, \tag{46}$$

where $\delta X = (\delta V, \delta w)^T$. Fig. 6 shows the maximal Lyapunov exponent associated with the tongue structure shown in Fig. 5.

For the parameter values we have investigated, chaotic behaviour is rare. However, by increasing b and V_r, and decreasing τ_w, we are able to obtain chaotic behavior, as seen in Fig. 7. Note that for these parameter values, the reset value V_r is greater than V_T (often resulting in bursting behavior), and the system is qualitatively similar to that studied by [Coombes *et al.*, 2012].

8. Discussion

In this paper we studied the periodically-forced piecewise-linear variant of the adaptive exponential integrate-and-fire neuron. The piecewise-linear nature of the model allowed us to explicitly construct arbitrary solutions, and in particular, $p : q$ mode-locked ones, in which the neuron fires p times for every q periods of the forcing. Such solutions satisfy a number of simultaneous nonlinear algebraic equations, which can be solved using Newton's method; these solutions can be numerically continued as parameters are varied. We derived expressions for the stability of an arbitrary orbit which has two components: one from the smooth flow between firings, and one from the discontinuity at firing. This enabled us to detect period-doubling and saddle-node bifurcations of mode-locked orbits. An interesting aspect of this model, that we are not aware of occurring elsewhere, is that if the amplitude of periodic forcing is sufficiently large, solutions can enter different regions of phase space multiple times between firing. Significant parts of the boundaries of Arnol'd tongues are defined by saddle-node bifurcations of such orbits.

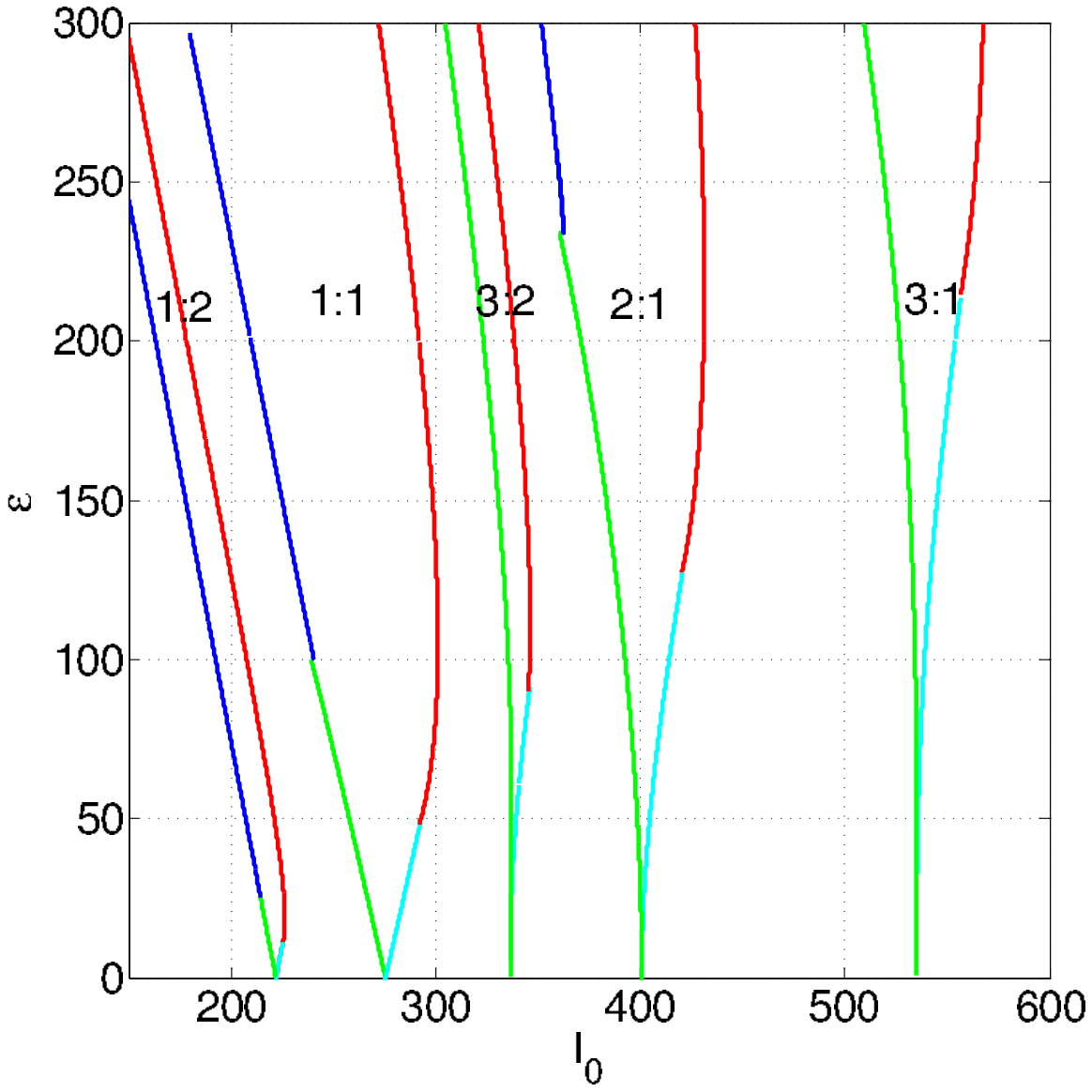

Figure 5. Tongue structure of phase locking solutions is shown in ε vs I_0 parameter space. Each boundary shows where a phase-locked solution goes through a specific bifurcation. Blue indicates a period-doubling bifurcation, green and cyan indicate saddle-node bifurcations, and red indicates a saddle-node bifurcation for solutions which cross $V = V_T$ three times betwen firings. Parameters as in Fig. 4.

We also observed similar tongue structures when the spike triggered adaptation parameter, b, was increased (not shown). More specifically, while similar tongue structures are maintained, the associated phase locked solutions are shifted to higher values of I_0 (in the ε vs I_0 plane), as the parameter b is increased. This is consistent with the findings shown in [Ladenbauer *et al.*, 2012] that higher values of input current I_0 are required to maintain the same spiking frequency, when higher values of b are used.

For analytical tractability the subthreshold adaptation parameter, a, is set at $a = 0$ in this study. Numerical studies (not shown) also show that tongue structures shift to the right (in the ε vs I_0 plane) as this parameter is increased. This again agrees with finding shown in [Ladenbauer *et al.*, 2012] that higher values of input current I_0 are necessary to produce the same spiking frequency, when higher values of a are used.

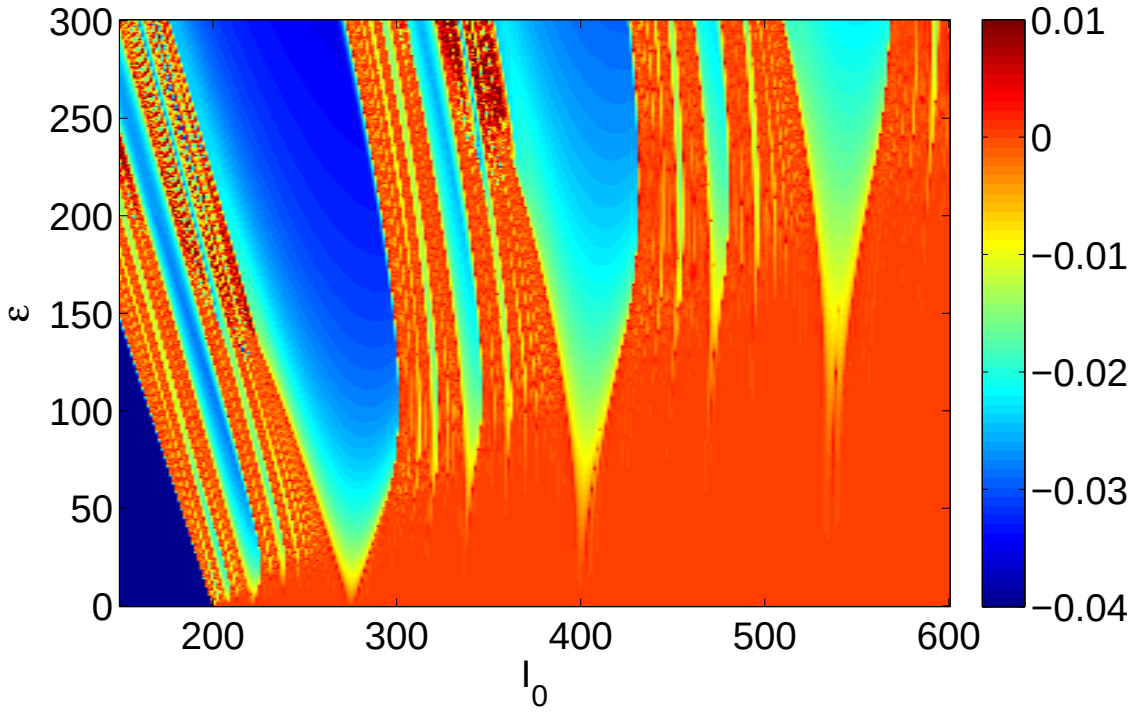

Figure 6. Maximal Lyapunov exponent. Parameters as in Fig. 4.

Acknowledgments

We would like to thank Stephen Coombes for the initial discussion of this study and his valuable input. LS is supported by National Science Foundation (DMS-1226282).

Appendix: Derivation for orbits crossing $V = V_T$ three times

Here we derive the equations governing the $1:1$ solution which crosses $V = V_T$ three times per period. Initially, at time t_n, $w = w_0$ and $V = V_r$. Then

$$X(t_n+T_1) = \begin{pmatrix} V_T \\ w_0 e^{-T_1/\tau_w} \end{pmatrix} = G^1(T_1)\begin{pmatrix} V_r \\ w_0 \end{pmatrix} + \int_0^{T_1} G^1(s) g_1(t_n+T_1-s)ds, \tag{47}$$

$$\begin{aligned} X(t_n+T_1+T_2) &= \begin{pmatrix} V_T \\ w_0 e^{-(T_1+T_2)/\tau_w} \end{pmatrix} \\ &= G^2(T_2)\begin{pmatrix} V_T \\ w_0 e^{-T_1/\tau_w} \end{pmatrix} + \int_0^{T_2} G^2(s) g_2(t_n+T_1+T_2-s)ds, \end{aligned} \tag{48}$$

$$\begin{aligned} X(t_n+T_1+T_2+T_3) &= \begin{pmatrix} V_T \\ w_0 e^{-(T_1+T_2+T_3)/\tau_w} \end{pmatrix} \\ &= G^1(T_3)\begin{pmatrix} V_T \\ w_0 e^{-(T_1+T_2)/\tau_w} \end{pmatrix} + \int_0^{T_3} G^1(s) g_1(t_n+T_1+T_2+T_3-s)ds, \end{aligned} \tag{49}$$

and

$$\begin{aligned} X(t_n+T_1+T_2+T_3+T_4) &= \begin{pmatrix} V_{th} \\ w_0 e^{-(T_1+T_2+T_3+T_4)/\tau_w} \end{pmatrix} \\ &= G^2(T_4)\begin{pmatrix} V_T \\ w_0 e^{-(T_1+T_2+T_3)/\tau_w} \end{pmatrix} + \int_0^{T_4} G^2(s) g_2(t_n+T_1+T_2+T_3+T_4-s)ds. \end{aligned} \tag{50}$$

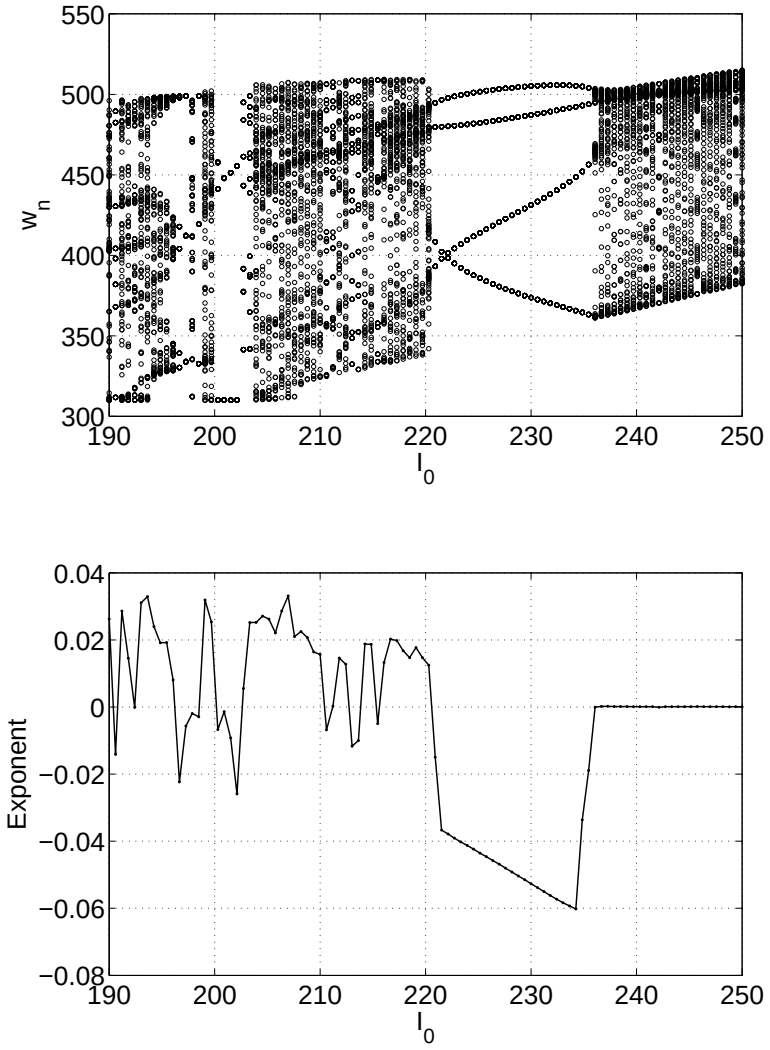

Figure 7. Top: value of w after each firing. Bottom: maximal Lyapunov exponent. Parameters: $b = 310\ pA, V_r = -40\ mV, V_{th} = -36\ mV, \tau_w = 5\ ms, C = 100\ pF, \Delta_T = 3\ mV, g_L = 10\ nS, V_T = -50\ mV, \omega = 0.04, \varepsilon = 60, E_L = -70\ mV$.

As above, $w_0 = e^{-T/\tau_w} w_0 + b$, and $I(t) = I_0 + \varepsilon \sin(\Omega t)$. Given w_0 and t_n, the next firing time, t_{n+1}, is found as follows. Find T_1 by solving $f_1(T_1; t_n, w_n) = 0$, where

$$\begin{aligned} f_1(T_1; t_n, w_0) &= -V_T + G^1_{11}(T_1)V_r + G^1_{12}(T_1)w_0 + \frac{1}{C}\int_0^{T_1} G^1_{11}(s)[I(t_n + T_1 - s) + g_L E_L]ds \\ &= -V_T + e^{-g_L T_1/C}V_r + k_1(e^{-g_L T_1/C} - e^{-T_1/\tau_w})w_0 + (1/C)P(-g_L/C, t_n, T_1, g_L E_L), \end{aligned} \tag{51}$$

and P is given by (43). We then find T_2 by solving $f_2(T_2; T_1, t_n, w_0) = 0$, where

$$\begin{aligned} f_2(T_2; T_1, t_n, w_0) =& -V_T + G^2_{11}(T_2)V_T + G^2_{12}(T_2)w_0 e^{-T_1/\tau_w} \\ &+ \frac{1}{C}\int_0^{T_2} G^2_{11}(s)[I(t_n + T_1 + T_2 - s) - g_L \Delta_T E]ds \\ =& -V_T + e^{g_L \Delta_T T_2/C}V_T + k_2(e^{g_L \Delta_T T_2/C} - e^{-T_2/\tau_w})w_0 e^{-T_1/\tau_w} \\ &+ (1/C)P(g_L \Delta_T/C, t_n + T_1, T_2, -g_L \Delta_T E). \end{aligned} \tag{52}$$

We find T_3 by solving $f_3(T_3; T_2, T_1, t_n, w_0) = 0$, where

$$\begin{aligned} f_3(T_3; T_2, T_1, t_n, w_0) =& - V_T + G^1_{11}(T_3)V_T + G^1_{12}(T_3)w_0 e^{-(T_1+T_2)/\tau_w} \\ &+ \frac{1}{C}\int_0^{T_3} G^1_{11}(s)[I(t_n + T_1 + T_2 + T_3 - s) + g_L E_L]ds \\ =& - V_T + e^{-g_L T_3/C}V_T + k_1(e^{-g_L T_3/C} - e^{-T_3/\tau_w})w_0 e^{-(T_1+T_2)/\tau_w} \\ &+ (1/C)P(-g_L/C, t_n + T_1 + T_2, T_3, g_L E_L). \end{aligned} \tag{53}$$

We finally find T_4 by solving $f_4(T_4; T_3, T_2, T_1, t_n, w_0) = 0$, where

$$\begin{aligned} f_4(T_4; T_3, T_2, T_1, t_n, w_0) =& - V_{th} + G^2_{11}(T_4)V_T + G^2_{12}(T_4)w_0 e^{-(T_1+T_2+T_3)/\tau_w} \\ &+ \frac{1}{C}\int_0^{T_4} G^2_{11}(s)[I(t_n + T_1 + T_2 + T_3 + T_4 - s) - g_L \Delta_T E]ds \\ =& - V_{th} + e^{g_L \Delta_T T_4/C}V_T + k_2(e^{g_L \Delta_T T_4/C} - e^{-T_4/\tau_w})w_0 e^{-(T_1+T_2+T_3)/\tau_w} \\ &+ (1/C)P(g_L \Delta_T/C, t_n + T_1 + T_2 + T_3, T_4, -g_L \Delta_T E). \end{aligned} \tag{54}$$

Then $t_{n+1} = t_n + T_1 + T_2 + T_3 + T_4$. In terms of phases, for the $1:1$ locked orbit, we write $t_n = (n + \phi_0)T$ and successively solve

$$f_1(T_1; \phi_0 T, w_0) = 0, \tag{55}$$
$$f_2(T_2; T_1, \phi_0 T, w_0) = 0, \tag{56}$$
$$f_3(T_3; T_2, T_1, \phi_0 T, w_0) = 0, \tag{57}$$
$$f_4(T_4; T_3, T_2, T_1, \phi_0 T, w_0) = 0. \tag{58}$$

for $T_1, \ldots T_4$. The correct value of ϕ_0 is the one for which $T_1 + T_2 + T_3 + T_4 - T = 0$.

References

Alijani, A. K. [2009] "Mode locking in a periodically forced resonate-and-fire neuron model," *Phys. Rev. E* **80**, 051922, doi:10.1103/PhysRevE.80.051922.

Brderle, D., Petrovici, M., Vogginger, B., Ehrlich, M., Pfeil, M., Millner, M. & et al. [2011] "A comprehensive workflow for general-purpose neural modeling with highly configurable neuromorphic hardware systems," *Biol. Cybern.* **104**, 263–296.

Brette, R. & Gerstner, W. [2005] "Adaptive exponential integrate-and-fire model as an effective description of neuronal activity," *J. Neurophysiol.* **94**, 3637–42, doi:10.1152/jn.00686.2005.

Chacron, M. J., Longtin, A. & Pakdaman, K. [2004] "Chaotic firing in the sinusoidally forced leaky integrate-and-fire model with threshold fatigue," *Phys. D: Nonlinear Phenomena* **192**, 138 – 160, doi:10.1016/j.physd.2003.12.009.

Clopath, C., Jolivet, R., Rauch, a., Luscher, H. & Gerstner, W. [2007] "Predicting neuronal activity with simple models of the threshold type: Adaptive exponential integrate-and-fire model with two compartments," *Neurocomputing* **70**, 1668–1673.

Coombes, S. [1999] "Liapunov exponents and mode-locked solutions for integrate-and-fire dynamical systems," *Phys. Lett. A* **255**, 49–57.

Coombes, S. & Bressloff, P. [1999] "Mode locking and arnold tongues in integrate-and-fire neural oscillators," *Phys. Rev. E* **60**, 2086.

Coombes, S., Owen, M. R. & Smith, G. D. [2001] "Mode locking in a periodically forced integrate-and-fire-or-burst neuron model," *Phys. Rev. E* **64**, 041914.

Coombes, S., Thul, R. & Wedgwood, K. C. A. [2012] "Nonsmooth dynamics in spiking neuron models," *Phys. D* **241**, 2042 – 2057.

Coombes, S. & Zachariou, M. [2009] "Gap junctions and emergent rhythms," *Springer Series in Computational Neuroscience: Coherent Behavior in Neuronal Networks (Ed.: Josic, Rubin, Matias, Romo)* **3**, 77–94.

Destexhe, A. [2009] "Self-sustained asynchronous irregular states and up-down states in thalamic, cortical and thalamocortical networks of nonlinear integrate-and-fire neurons," *J. Comput. Neurosci.* **27**, 493–506, doi:10.1007/s10827-009-0164-4.

Ermentrout, B., Beverlin, B. & Netoff, T. [2011] *PRCs in neuroscience: theory, experiment and analysis: Phase response curves to measure ion channel effects on neurons* (Springer).

Ermentrout, B., Pascal, M. & Gutkin, B. [2001] "The effects of spike frequency adaptation and negative feedback on the synchronization of neural oscillators," *Neural. Comput.* **13**, 1285–310.

Gerstner, W. & Brette, R. [2009] "Adaptive exponential integrate-and-fire model," *Scholarpedia* **4**, 8427.

Jeong, H. & Gutkin, B. [2007] "Synchrony of neuronal oscillations controlled by gabaergic reversal potentials," *Neural. comput.* **19**, 706–29.

Jolivet, R., Schurmann, F., Berger, T. K., Naud, R., Gerstner, W. & Roth, A. [2008] "The quantitative single-neuron modeling competition," *Biol. Cybern.* **99**, 417–26.

Karbowski, J. & Kopell, N. [2000] "Multispikes and synchronization in a large neural network with temporal delays," *Neural. comput.* **12**, 1573–1606.

Knight, B. W. [1972] "The relationship between the firing rate of a single neuron and the level of activity in a population of neurons. experimental evidence for resonant enhancement in the population response," *J. Gen. Physiol.* **59**, 767–78.

Koch, C. [1999] *Biophysics of Computation: Information Processing in Single Neurons*, Vol. 428 (Oxford University Press).

Ladenbauer, J., Augustin, M., Shiau, L. & Obermayer, K. [2012] "Impact of adaptation currents on synchronization properties of coupled exponential integrate-and-fire neurons," *PLoS Comput. Biol.* **8(4): e1002478.**, doi: 10.1371 /journal.pcbi.1002478.

Laing, C. R. & Coombes, S. [2005] "Mode locking in a periodically forced ghostbursting neuron model," *Int. J. Bifurcat. Chaos* **15**, 1433–1444.

McCormick, D. & Huguenard, J. [1992] "Simulation of the currents involved in rhythmic oscillations in thalamic relay neurons," *J. Neruhysiol.* **68**, 1384–1395.

Moller, A. [1983] "Frequency selectivity of phase locking of complex sounds in the auditory nerve of the rat," *Hear. Res.* **11**, 267–284.

Naud, R., Marcille, N., Clopath, C. & Gerstner, W. [2008] "Firing patterns in the adaptive exponential integrate-and-fire model." *Biol. Cybern.* **99**, 335–47, doi:10.1007/s00422-008-0264-7.

Rieke, F., Warland, D., De Ruyter Van Steveninck, R. & Bialek, W. [1997] *Spikes: Exploring the Neural Code* (MIT Press).

Schultheiss, N. W., Prinz, A. A. & Butera, R. J. [2011] *Phase Response Curves in Neuroscience: Theory, Experiment, and Analysis* (Springer Verlag).

Smith, G. D., Cox, C. L., Sherman, S. M. & Rinzel, J. [2000] "Fourier analysis of sinusoidally driven thalamocortical relay neurons and a minimal integrate-and-fire-or-burst model." *J. of Neurophysiol.* **83**, 588–610.

Svensson, C. & Coombes, S. [2009] "Mode locking in a spatially extended neuron model: active soma and compartmental tree," *Int. J. Bifurcat. Chaos* **19**, 2597–2607.

Tonnelier, A. [2002] "The mckean's caricature of the fitzhugh-nagumo model i. the space-clamped system," *SIAM J. Appl. Math.* **63**, pp. 459–484.

Touboul, J. & Brette, R. [2008] "Dynamics and bifurcations of the adaptive exponential integrate-and-fire model," *Biol. Cybern.* **99**, 319–34, doi:10.1007/s00422-008-0267-4.